

# Effect of Mechanical Constraint on Domain Reorientation in Predominantly {111}-Textured Lead Zirconate Titanate Films

Giovanni Esteves,<sup>‡</sup> Margeaux Wallace,<sup>§</sup> Raegan Johnson-Wilke,<sup>§</sup> Chris M. Fancher,<sup>‡</sup> Rudeger H. T. Wilke,<sup>§</sup> Susan Trolier-McKinstry,<sup>§</sup> and Jacob L. Jones<sup>‡,†</sup>

<sup>‡</sup>Department of Materials Science and Engineering, North Carolina State University, Raleigh, North Carolina 27695

§Department of Materials Science and Engineering, The Pennsylvania State University, University Park, Pennsylvania 16802

Ferroelectric/ferroelastic domain reorientation was measured in 2.0 µm thick tetragonal {111}-textured PbZr<sub>0.30</sub>Ti<sub>0.70</sub>O<sub>3</sub> thin films using synchrotron X-ray diffraction (XRD). Lattice strain from the peak shift in the 111 Bragg reflection and domain reorientation were quantified as a function of applied electric field amplitude. Domain reorientation was quantified through the intensity exchange between the 112 and 211 Bragg reflections. Results from three different film types are reported: dense films that are clamped to the substrate (as-processed), dense films that are partially released from the substrate, and films with 3% volume porosity. The highest amount of domain reorientation is observed in grains that are misoriented with respect to the {111} preferred (domain engineered) orientation. Relative to the clamped films, films that were released from the substrate or had porosity exhibited neither significant enhancement in domain reorientation nor in 111 lattice strain. In contrast, similar experiments on {100}-textured and randomly oriented films showed significant enhancement in domain reorientation in released and porous films. Therefore, {111}textured films are less susceptible to changes in properties due to mechanical constraints because there is overall less domain reorientation in {111} films than in {100} films.

#### I. Introduction

L ead zirconate titanate (PZT) is a ferroelectric material used in a wide variety of applications that include sensors, actuators, microelectromechanical systems (MEMS), and ultrasound transducers. Ferroelectric materials have domain structures consisting of regions of (almost) uniform polarization that are separated by domain walls. Upon applying an electric field, domain reorientation occurs via domain wall motion. Thus, the piezoelectric response of ferroelectric materials is comprised of two major contributions; (1) the intrinsic piezoelectric effect and (2) extrinsic contributions associated with domain wall or phase boundary motion. The large piezoelectric coefficients in soft (donor-doped) bulk ferroelectric ceramics results from a large extrinsic contribution (up to 75% of the total piezoelectric response). 4

In tetragonal perovskite ferroelectrics, the polarization can be parallel to any of the six pseudocubic <001> directions of the unit cell [Fig. 1(a)]. Reorientation in which the polarization changes orientation by an angle of ~90° is referred to as 90° ferroelectric/ferroelastic domain reorientation, e.g., reorienting from either polarization states 1, 2, 4, or 5 to state 3.

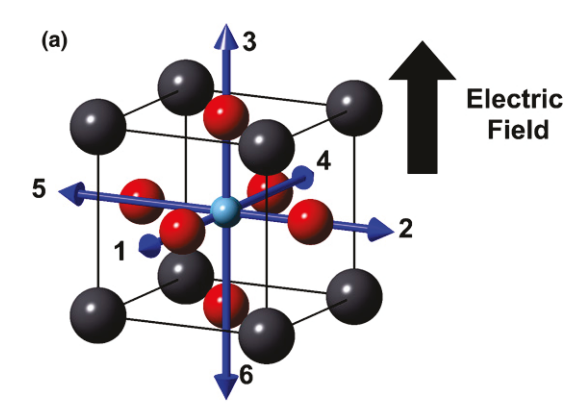
Manuscript No. 37699. Received October 27, 2015; approved January 11, 2016. Author to whom correspondence should be addressed. e-mail: JacobJones@ncsu.edu This domain reorientation is accompanied by switching of the spontaneous ferroelastic strain. Figure 1(b) describes a situation in which the electric field direction is parallel to the pseudocubic <111>. In this situation, domain states 1, 2, and 3 of a tetragonal cell are at equal angles relative to the applied electric field direction and can be referred to as "domain engineered". In this case, no ferroelectric/ferroelastic reorientation is expected upon application of an electric field of a prepoled sample.

Ferroelectric films with preferred orientation (texture) can be considered model systems to describe the behavior of a variety of textured materials, e.g., bulk piezoceramics produced by templated grain growth. The amount of domain reorientation in a polycrystalline ferroelectric is dependent on the preferred orientation (texture) of the material. 6-8 Tetragonal PZT thin films have two commonly studied textures: {001} and {111}. Depending on the texture of the material, the ferroelectric film can be used in different applications. For example, {001} oriented films have potential uses in actuators, sensors, and MEMS due to their high piezoelectric response. {111} oriented films have stable properties and exhibit large remanent polarizations  $(P_r)$ , which make them an attractive candidate for ferroelectric random access memory (FeRAM). [111] -textured tetragonal films are also reported to retain their properties to small film thicknesses, which is useful for applications mandating low voltage.12

The durability of high-performance PZT films depends on the crystallographic anisotropy of the piezoelectric and elastic properties, which is often maximized near phase boundaries. In a representative PZT film near the morphotrophic phase boundary (MPB), the piezoelectric effect resulting from an electric field of 100 kV/cm was shown to generate an in-plane stress close to 200 MPa. <sup>13</sup> This stress is a result of the large, negative transverse coefficient,  $e_{31,f}$ , imposing a large tensile piezoelectric stress in the film. These large stresses would be exacerbated by the presence of misoriented grains, and so would be expected to reduce reliability due to cracking and mechanical failure. Even in as-processed films before application of electric field, the stress state of the film is influenced by factors such as processing conditions, choice of substrate, aspect ratio of the crystal structure, and microstructure of the film.

The overall piezoelectric response of ferroelectric PZT thin films is also significantly reduced relative to bulk materials. <sup>14,15</sup> A variety of factors have been shown to contribute to this reduction: substrate clamping, limited domain wall mobility, defects, and small grain sizes. <sup>15–18</sup> As-processed PZT films grown on silicon substrates tend to be under tensile stress due to difference in the coefficient of thermal expansion between the film and the substrate. <sup>19</sup> As a result of this tensile stress, the polarization axis is predominantly in the plane of the film. This tensile stress also makes it difficult for domains to reorient during applied electric fields because

G. L. Brennecka—contributing editor



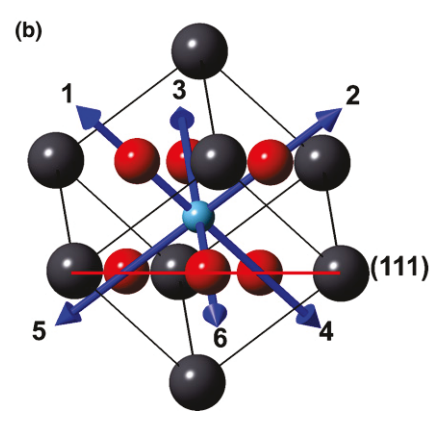


**Fig. 1.** (a) Shows the six polarization states in a tetragonal perovskite unit cell, this is also the predominant unit cell orientation for  $\{001\}$ -textured films, and (b) unit cell oriented with (111) plane oriented horizontally which represents  $\{111\}$ -textured films. In (a and b) Gray atoms correspond to  $Pb^{2+}$ , red to  $O^{-2}$ , and cyan to  $Ti^{4+}/Zr^{4+}$ .

it creates a large energy barrier for domain reorientation.  $^{20}$  However, Wallace et al.  $^{14}$  showed that the removal of  $\sim\!75\%$  of the mechanical boundary constraints imposed by the substrate resulted in a sixfold increase in domain reorientation relative to a fully clamped film. Additionally, porous  $\{001\}$ -textured PZT films also show an increased domain reorientation relative to dense  $\{001\}$ -textured PZT films.  $^{21}$  The increase in domain reorientation due to porosity was suggested to involve two possible mechanisms: (1) local enhancement of the electric fields near a pore, or (2) reduction in the film clamping due to a reduction in the film stiffness as a result of porosity.

Previous reports suggest that certain properties of {111} oriented tetragonal PZT films are less susceptible to substrate clamping than those in films with different textures. 11,22 Kuwabara et al. 11 studied the polarization saturation response of {111}-textured and epitaxial tetragonal PZT films using different substrates. Silicon and strontium titanate substrates were used to introduce either a tensile or compressive stress in the PZT films. From this study, the authors found that the properties do not drastically depend on the strain state imposed by the substrate. Furthermore, Yamada et al.<sup>22</sup> reported negligible substrate clamping in {111} tetragonal epitaxial PZT films compared to {001} epitaxial films. Yamada et al.<sup>22</sup> calculated the strain from shifts in the Bragg reflections for {001} and {111} epitaxial films, and compared those to values calculated from simulations of the same films but released from the substrate. The experimental {111} epitaxial film strain matched the theoretical model while the {001} epitaxial films deviated from the model; this comparison suggest that substrate clamping had a larger effect on {001} oriented films.

The work described above shows that piezoelectric properties of ferroelectric thin films can be significantly influenced by both the texture of the ferroelectric material itself (i.e., domain engineering of the texture) as well as the mechanical constraint on the film (e.g., clamping of the film to the substrate). In the present work, 2 µm thick films of PbZr<sub>0.3</sub>Ti<sub>0.70</sub>O<sub>3</sub> with {111} texture were used to further delineate the roles of the texture and mechanical constraint mechanisms on domain reorientation. XRD is a useful technique to measure domain reorientation during electric field application, and has been applied in the past to measure changes in both bulk and thin film ferroelectrics. <sup>17,21,23–25</sup>

## II. Experimental Procedure

#### (1) Sample Fabrication

Thin films of PbZr<sub>0.30</sub>Ti<sub>0.70</sub>O<sub>3</sub> (PZT 30/70) with 1% manganese were deposited via chemical solution deposition onto platinized silicon substrates. Details of the sample synthesis are described elsewhere<sup>26,27</sup> and a brief description is provided here. A solution of PZT 30/70 containing 10% excess PbO was spin coated onto commercial substrates from Nova Electronics Materials (Flower Mound, TX), which consist of 1500 Å of Pt/200 Å of  $TiO_2/10~000$  Å of  $SiO_2/Si$ . The films were then pyrolyzed at 250°C and 400°C for 5 min to ensure high-density films<sup>21</sup> and then were crystallized in a rapid thermal annealing furnace at 700°C for 1 min. This process was repeated until a 2 µm thickness was reached. The synthesized films were found to be crack free and dense. The released film was partially released from the substrate by creating circular diaphragms in the electrode region with 75% of the substrate removed. This process is described elsewhere. 14 Porous films were fabricated in a similar way to the clamped, dense released films, with the only difference being reducing the pyrolysis bake times to 1 min to lower the density. The amount of porosity in the film was estimated to be ~3 vol%, based on spectroscopic ellipsometry measurements, as described in Ref. [21]. Table I summarizes the electrical properties of the films.

The microstructure of the PZT films was characterized using a field-emission scanning electron microscope (FESEM) and XRD. Plan view and cross-section images were obtained for clamped, released, and porous films using an FESEM; these images are shown in Fig. S1 available online as supplemental material. The clamped, released, and porous films were verified to have a predominant {111} texture using synchrotron XRD data. Based on these results, calculated Lotgering factors for the clamped, released, and porous films were 80%, 80%, and 81%, respectively.

#### (2) X-ray Measurements and Analysis

XRD measurements were conducted at beamline 11-ID-C of the Advanced Photon Source at Argonne National Laboratory. The X-ray beam used for these measurements was 500  $\mu m$  wide by 100  $\mu m$  tall with a beam energy of ~115 keV (0.10801 Å). PZT thin films were mounted on a custom-built stage designed to house the sample and electrical probes. An incidence angle of 1° in  $\theta$  was used to increase the volume of irradiated material. Thus, the beam footprint on the sample was 500  $\mu m$  wide by ~5.6 mm in length. Electric fields were applied using electrical probes and a Keithley 2410C 1100 V source meter.

Table I. Electrical Properties of Synthesized PZT(30/70)
Films

	$P_r \; (\mu C/cm^2)$	$V_{c}(V)$	Leakage (μA/cm <sup>2</sup> )	$\epsilon_r$	Loss
Clamped/ Released	34	12.1	0.04237	477	0.0168
Porous	30.5	12	0.02	467	0.0077

Diffraction measurements were performed in situ with application of an external electric field. For the dense films (i.e., clamped and released), each sample was cycled through two voltage cycles. The first voltage cycle started at 0 V and increased in steps of 0.25  $V_c$ , where  $V_c$  is the coercive voltage ( $\sim$ 12 V), up to 1.5 V<sub>c</sub> at which point the voltage decreased in steps of 0.5 V<sub>c</sub>. The second voltage cycle was measured up to 3  $V_c$  in steps of 0.5  $V_c$  and back down to 0 V in steps of  $V_c$ . Only one voltage cycle was measured for the porous film. This voltage cycle closely matches the second voltage cycle of the clamped and released films with the exception of a steeper decrease in voltage, 1.5  $V_c$ , once 3  $V_c$  was reached. At each voltage step, diffraction patterns were measured for 210 s, and the capacitance and loss of the films were measured at the start and end of every cycle to help determine if permanent degradation had occurred.

Measured 2D diffraction images were reduced into intensity versus  $2\theta$  patterns using the  $Fit2D^{28}$  software. The X-ray beam center, sample-to-detector distance, and detector orthogonality were calibrated within Fit2D using a standard reference material CeO<sub>2</sub> (NIST 674b). Two primary sections from the 2D image were chosen for integration. The first sector was a 20° section centered at the vertical section of the image. This sector represents scattering vectors that are approximately parallel to the electric field and is denoted  $\chi^{0^{\circ}}$ . The second sector was another 20° section centered 20° to the right from the vertical section of the 2D image. This sector represents scattering vectors that are 20° away from the electric field direction and is denoted  $\chi^{20^\circ}$ . Both of these sectors are highlighted in Fig. 2(b). After extracting 1D diffraction patterns from the 2D diffraction images, line-profile analysis was carried out using pseudo-Voigt functions. When peak fitting the 112 and 211 reflections, the mixing parameters of each pseudo-Voigt function, which weight the Gaussian and Lorentzian components, were constrained to be equal during the fitting procedure.

The extent of domain reorientation was calculated using the integrated intensity of the 112 and 211 reflections. While the 002 and 200 reflections have been used to quantify domain reorientation in prior work,  $^{14,24}$  the present work uses the 112 and 211 reflections because these reflections can characterize domain reorientation selectively in certain crystallographic orientations of interest to {111}-oriented films. In  $\chi^{20^{\circ}}$ , for example, the 112 and 211 reflections predominantly represent crystallographic orientations that are consistent with the preferred orientation of the film, i.e., the [111] parallel to the field direction [Fig. 1(b)]. The volume fraction

of domains aligned in a given sector ( $v_{112}$ ), can be determined using Eq. (1):

$$v_{112} = \frac{\frac{I_{112}}{I_{112}}}{\frac{I_{112}}{I_{122}} + 2\frac{I_{211}}{I_{112}}} \tag{1}$$

where  $I_{112}$  is the integrated intensity of the 112 reflection and  $I'_{112}$  is the reference intensity from a Powder Diffraction File<sup>TM</sup> for the 112 reflection ( $I'_{112} = 183, I'_{211} = 332$ ). The ratio of the reference intensities of a Powder Diffraction File<sup>TM</sup>,  $I'_{112}$ , and the intensities of the sample,  $I_{112}$ , are used to account for the difference in structure factors for 112 and 211 reflections. From the volume fraction of 112 domains, the fraction of domain reorientation ( $\eta_{112}$ ) can be calculated using Eq. (2). In Eq. (2),  $\nu_{112}^{0 \text{ field}}$  corresponds to the initial unpoled state of the film and  $\nu_{112}$  is at a nonzero voltage. By making the volume fraction relative to the volume fraction at zero field ( $\nu_{112}^{0 \text{ field}}$ ), Eq. (2) accounts for scenarios in which an initial domain orientation is present.

$$\eta_{112} = \nu_{112} - \nu_{112}^{0 \text{ field}} \tag{2}$$

The amount of electric field induced lattice strain obtained from the peak shift in the PZT 111 reflection, %  $\epsilon_{(111)}$ , was calculated for each voltage step. A pseudo-Voigt function was used to fit the PZT 111 reflection to obtain the peak position at each voltage step.

$$\% \, \varepsilon_{(111)} = \left(\frac{d_{(111)} - d_{(111)}^{0 \,\mathrm{V}}}{d_{(111)}^{0 \,\mathrm{V}}}\right) * 100 \tag{3}$$

In Eq. (3),  $d_{(111)}$  is the *d*-spacing of the PZT 111 reflection at a specified voltage, and  $d_{(111)}^{0\,V}$  is the *d*-spacing at 0 V. Values of %  $\epsilon_{(111)}$  yield information about the lattice strain of the film with respect to the displacement of the (111) plane. The value of % $\epsilon_{(111)}$  can be influenced by both the intrinsic piezoelectric effect and domain wall motion.<sup>30</sup>

#### III. Results and Discussion

The electric field-dependent diffraction data of the clamped film corresponding to sectors  $\chi^{0^\circ}$  and  $\chi^{20^\circ}$  are shown in Fig. 3. A larger intensity exchange between the 112 and 211 PZT reflections is observed in the  $\chi^{0^\circ}$  sector [Fig. 3(a)],

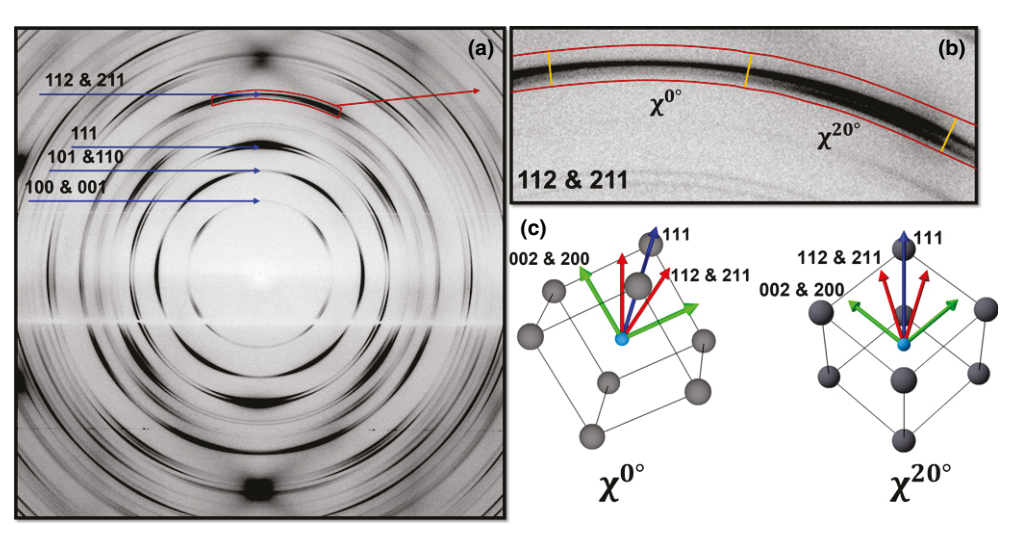


Fig. 2. (a) 2D diffraction image of PZT thin film with reflections labeled, (b) integration areas chosen for data extraction the  $\chi^{0^{\circ}}$  and  $\chi^{20^{\circ}}$  sections represents diffraction signals that have scattering vectors equal to the angle of the labeled section, and (c) represents the crystal structure that gives rise to the signal seen in (b) for both sections. The poles for certain planes are labeled for visualization.

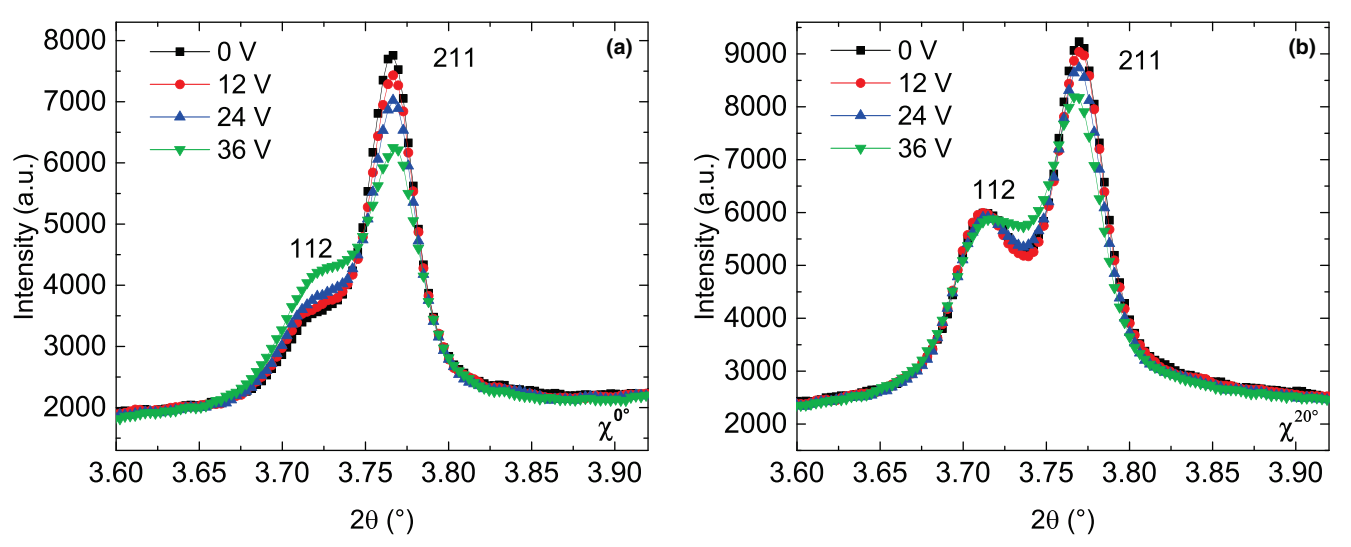


Fig. 3. (a) Diffraction signal from  $\chi^{0^{\circ}}$  for the 112 and 211 reflections, and (b) Diffraction signal from  $\chi^{20^{\circ}}$ .

relative to the data for the  $\chi^{20^\circ}$  sector [Fig. 3(b)]. The smaller intensity exchange between the 112 and 211 reflections for the  $\chi^{20^\circ}$  sector indicates that less 90° ferroelectric/ferroelastic domain reorientation is occurring relative to the  $\chi^{0^\circ}$  sector. Bassiri–Gharb et al. suggested that PZT {111}-textured films have lower  $d_{33}$  values because they cannot benefit from non-180° domain reorientation. Figure 3 shows a measureable amount of domain reorientation in both the  $\chi^{0^\circ}$  and  $\chi^{20^\circ}$  sectors, though its influence on properties such as  $d_{33}$  is not yet known.

The integrated intensities of the 112 and 211 reflection were used to quantify domain reorientation using Eq. (2), resulting in  $\eta_{112}$  values for each pattern, seen in Fig. 4. Figures 4 (a and b) shows the fraction of domain reorientation,  $\eta_{112}$ , in the  $\chi^{0^\circ}$  and  $\chi^{20^\circ}$  sectors, respectively, as a function of electric field amplitude. The  $\chi^{0^\circ}$  sector shows a significant amount of domain reorientation in all three film typesclamped, porous, and released. Grains that give rise to scattering intensities in the  $\chi^{0^{\circ}}$  sector have an orientation that is not part of the dominant texture component (i.e., these grains do not have their (111) parallel to the surface of the film). Figure 2 summarizes the integration areas chosen for data extraction as well as the predominant unit cell orientation that corresponds to the signal that is being measured at each  $\chi$  sector. Figure 2(c) shows a  $\chi^{0^{\circ}}$  unit cell orientation with the (112) plane parallel to the film. The subset of misoriented grains is suggested to have a {112} texture (or almost so) and the data shows that domain reorientation can occur within these grains. In this orientation, the 002 pole is more closely aligned to the electric field direction than the 200 or 020 pole, which means 90° ferroelectric/ferroelastic switching is possible, and explains why domain reorientation is seen in the data shown in Fig. 4(a).

A significant reduction in domain reorientation is seen in Fig. 4(b) relative to Fig. 4(a) because more {111} oriented grains are probed in this region. For the sake of simplicity, a "grain orientation" will be referred to as the orientation of a grain without considering the domain structure, e.g., by referring to the pseudocubic unit cell. If the  $\chi^{20^{\circ}}$  sector only sampled grain orientations in the primary film orientation, i.e., {111} oriented, minimal or no domain reorientation would be expected in this sector. The small amount of domain reorientation detected in this sector can be attributed to two factors. First, the integration range of the  $\chi^{20^{\circ}}$  sector is from 60° to 80°, which means that the integrated 1D XRD patterns resulting from this sector include scattering from misoriented grain orientations. However, even if the sector integration range could be reduced infinitesimally, some misoriented grains would still diffract in this region and

contribute to scattering in the  $\chi^{20^\circ}$  sector. This is the second effect and is described as follows. Consider a grain orientation that is consistent with the film texture, i.e., 111 orientation. The pseudocubic 112 pole would be oriented at an angle of ~19.5° from the sample normal (included in the sector integration range for  $\chi^{20^\circ}$ ). Not only does this grain orientation satisfy the Bragg condition for diffraction in the  $\chi^{20^\circ}$  sector, but numerous other grain orientations can satisfy the Bragg condition as well. These other grain orientations can be visualized by rotating the {111} dominant grain orientation about the 112 pole. This would allow for a diffraction signal from the 112 and 211 to appear at  $\chi^{20^\circ}$ , but have a grain orientation that is not {111} oriented; thus, allowing for domain reorientation to occur. The superposition of both misoriented and oriented grains is responsible for the 8% domain reorientation value seen at  $\chi^{20^\circ}$  at 36 V.

From Figs. 5 (a and b), the %  $\epsilon_{(111)}$  were calculated by using the shift in the PZT 111 reflection at specified voltages for all film types. Values of %  $\epsilon_{(111)}$  provide information on the electric field-induced strain exhibited by the material due to the effective piezoelectric effect. From Figs. 5 (a and b), the field-induced strain for the three different samples falls within error bars, which means that their electric fieldinduced lattice strain response is less susceptible to mechanical constraints than {100}-oriented films of the same thickness and composition. These results compare well with the trend in  $\eta_{112}$  values shown in Figs. 4 (a and b) for the three different film types and the strain values reported from Yamada et al.<sup>22</sup> for a {111} epitaxial film. When referring to the PZT 111 reflection, the diffraction signal from  $\chi^{0^{\circ}}$  represents the diffraction signal of grains oriented with their (111) closely parallel to the sample surface, i.e., the predominant orientation of the films. In contrast, diffraction signal in the  $\chi^{20^{\circ}}$  sector from the 111 reflection is attributed to grains that are not {111} oriented. In the case of Fig. 5(a), the electric field induced lattice strain,  $\%\epsilon_{(111)}$ , measured from the  $\chi^0$ sector results from predominantly {111}-oriented grains while Fig. 5(b) shows %  $\epsilon_{(111)}$  from misoriented grains. The hysteretic effect shown in Fig. 5(a) indicates the presence of some domain reorientation in grains that are closely oriented to the predominant orientation of the film, which correlates with the result of Fig. 4(b) for  $\chi^{20^\circ}$ .

In the present work, the extent of domain reorientation depends more strongly on the actual grain orientation than on the mechanical constraints in predominantly  $\{111\}$ -oriented films. Figure 4 shows that domain reorientation is essentially unaffected by release via circular diaphragms, or via introduction of  $\sim 3$  vol% porosity. This result is different from that shown in  $\{001\}$ -textured tetragonal PZT films by

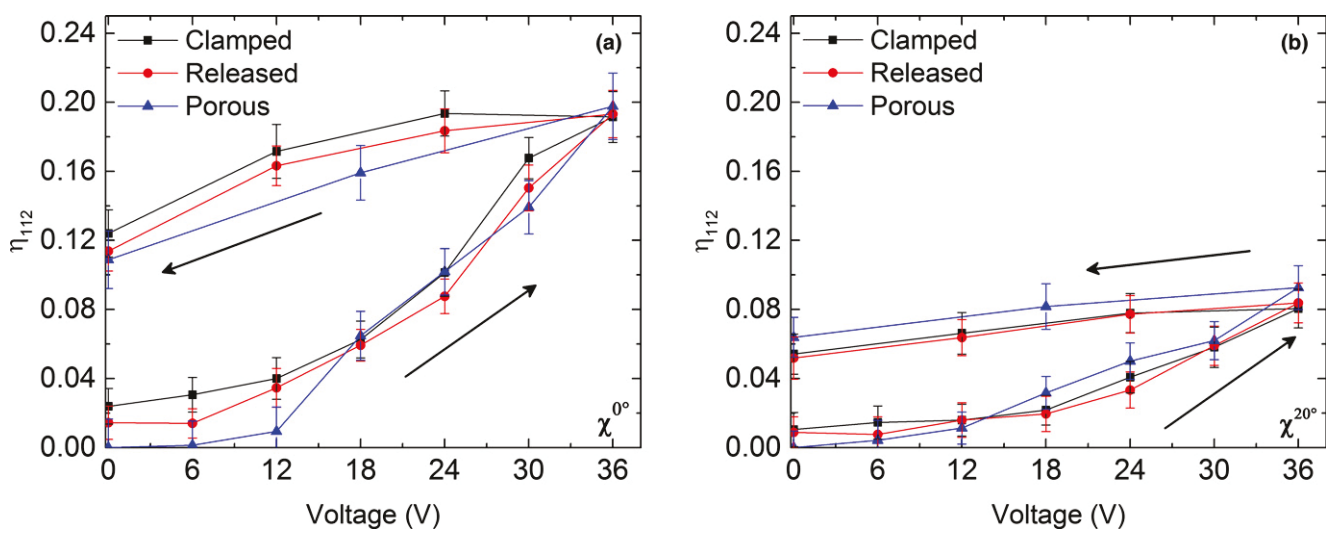


Fig. 4. (a) Amount of domain reorientation seen in  $\chi^{0^{\circ}}$  and (b) domain reorientation from  $\chi^{20^{\circ}}$ . The error bars for Fig. 4 were calculated using error propagation.

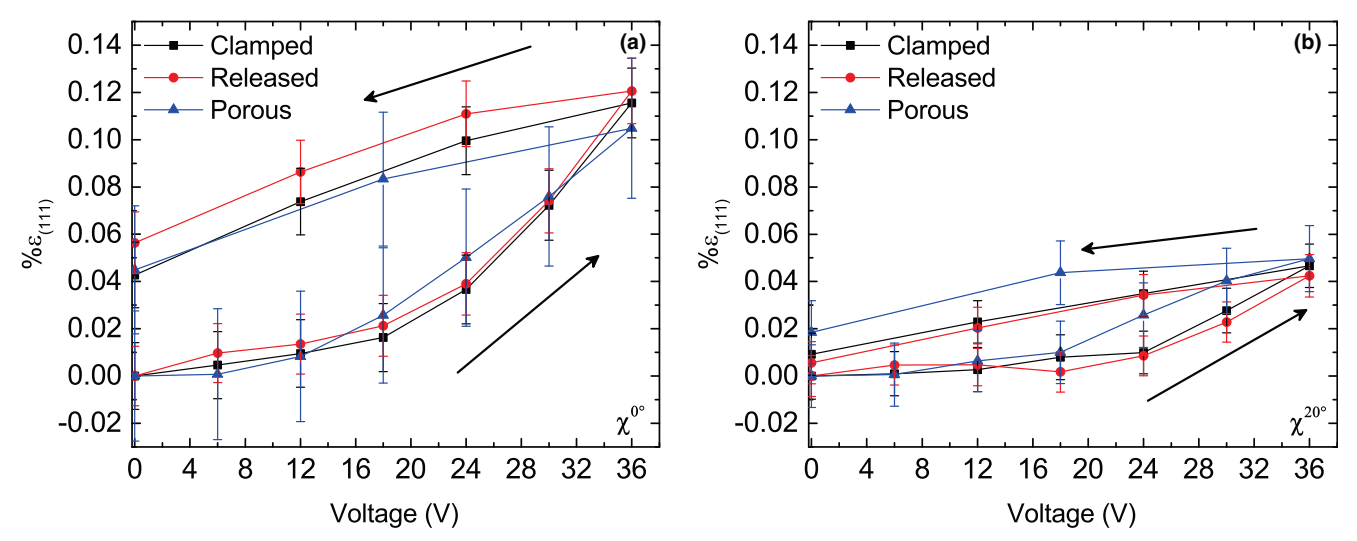


Fig. 5. (a) Shows the  $\%\epsilon_{(111)}$  for  $\chi^{0^\circ}$  as a function of voltage, and (b)  $\%\epsilon_{(111)}$  for the  $\chi^{20^\circ}$  as a function of voltage. The error bars for Fig. 5 were calculated using error propagation.

Wallace et al.<sup>14</sup> and Johnson-Wilke et al.,<sup>21</sup> in which released films (via slot-shaped structures) and porous films experienced much greater domain reorientation than in clamped films. The films in the present work have a different texture and geometry of release. {111}-textured tetragonal films are anticipated to be less susceptible to 90° ferroelectric/ferroelastic domain reorientation for the dominant grain orientation due to domain engineering. That said, the 90° ferroelectric/ferroelastic domain reorientation observed in these films for misoriented grains are neither affected by porosity nor elimination of the films-substrate mechanical interface. This could be a result of the volume fraction of misoriented grains being small compared to the domain engineered grain orientation. That is, the misoriented grains are probably constrained by the well-oriented matrix.

The differences in the geometry used to release the film is anticipated to significantly change the stress state of the film, which can affect the domain reorientation values and lead to differences between the film types. Therefore, the relative importance of the geometry of the mechanical release structure is currently under investigation via a combination of experimental measurements and finite element modeling. Preliminary work suggests that diaphragm structures experience higher levels of in-plane stress than those released from the

substrate via slots. This may explain, at least in part, the smaller degree of domain reorientation observed in the diaphragms of the current work relative to the slots characterized in prior work.

In PZT films that can undergo domain reorientation, an increase in domain reorientation leads to an increase in electric field-induced strain. When releasing or introducing porosity in a {001} film, applying an electric field enhances the domain reorientation, relative to a dense clamped film, which leads to an enhanced response. In the case of {111}textured grains, however, the domains are oriented such that switching from one domain state to another is not favorable. Although the films reported in this study exhibit domain reorientation due to misaligned grains, the volume fraction of the subset of misaligned grains is small compared to the overall volume of grains probed by XRD. Therefore, it is suggested that the influence of the substrate on ferroelastic switching is more important in films that can undergo substantial domain reorientation, i.e., mostly random, {001}or {110}-textured films.

The durability of high-performance ferroelectric films depends on their microstructure. Microcracking is a possible mechanism of failure for PZT films with high  $e_{31,f}$  coefficients, particularly for films that are electrically cycled or

subjected to electric fields for an extended period of time.<sup>13</sup> The results presented earlier demonstrated that the films consists of a dominant orientation [(111) parallel to the film], but also consists of a measurable fraction of grains that deviate from this orientation. The electric field-induced strain in these two different grain orientations would be expected to be different. The difference between strains from unique grain orientations can introduce microstresses within the film that act as crack initiation sites during electric field cycling. This, in turn, may lower the actuator lifetime [P. Muralt, *Personal Communication*, (2015)].

## IV. Conclusions

Synchrotron X-ray diffraction was used to measure the exchanges in intensity between the 112 and 211 reflections as well as the shift in 111 reflection as a function of applied field in 2 µm thick tetragonal PZT films. The domain reorientation and  $%\epsilon_{(111)}$  values are reported for three different types of predominantly {111}-textured PZT samples; clamped, released, and porous. The highest amount of domain reorientation was found in a subset of grain orientations that are misoriented relative to the dominant {111} texture orientation. The misorientation of grains relative to the dominant grain orientation is proposed to produce inhomogeneous strains throughout the film that can lead to microcracking during electrical loading. The amount of domain reorientation and %ε(111) measured for all three films provides evidence that the response of {111}-textured films is less susceptible to substrate clamping, and that their degree of orientation can govern the susceptibility to mechanical constraints. The results of this work suggest that there is a stronger dependence of texture of {111} PZT films on domain reorientation than that of mechanical constraints.

# Acknowledgments

The authors gratefully acknowledge support of this research from the U.S. National Science Foundation (DMR-1410907 and DMR-1409399), and a National Security Science and Engineering Faculty Fellowship (STM). This research used resources of the Advanced Photon Source, a U.S. Department of Energy (DOE) Office of Science User Facility operated for the DOE Office of Science by Argonne National Laboratory under Contract No. DE-AC02-06CH11357. The technical assistance of Rick Spence at beamline 11-ID-C is gratefully acknowledged. Additionally, the authors gratefully acknowledge Adarsh Rajashekhar for ellipsometry data collection and modeling.

# **Supporting Information**

Additional Supporting Information may be found in the online version of this article:

**Fig. S1.** (a) Cross-sectional view of clamped {111}-textured PZT film. (b) Plan view of {111}-clamped PZT film. (c) Cross section of porous {111} PZT film.

# References

- <sup>1</sup>P. G. Evans and R. J. Sichel-Tissot, "In Situ X-ray Characterization of Piezoelectric Ceramic Thin Films," J. Am. Ceram. Soc., **92** [1] 18–23 (2013).

  <sup>2</sup>M. Ahart, et al., "Origin of Morphotropic Phase Boundaries in Ferro-
- <sup>2</sup>M. Ahart, et al., "Origin of Morphotropic Phase Boundaries in Ferroelectrics," *Nature*, **451** [7178] 545–8 (2008).
- <sup>3</sup>N. Bassiri-Gharb, İ. Fujii, E. Hong, S. Trolier-McKinstry, D. V. Taylor, and D. Damjanovic, "Domain Wall Contributions to the Properties of Piezo-electric Thin Films," *J. Electroceram.*, **19** [1] 49–67 (2007).
- <sup>4</sup>Q. M. Zhang, H. Wang, N. Kim, and L. E. Cross, "Direct Evaluation of Domain-Wall and Intrinsic Contributions to the Dielectric and Piezoelectric Response and Their Temperature Dependence on Lead Zirconate–Titanate Ceramics," *J. Appl. Phys.*, **75** [1] 454–9 (1994).

- <sup>5</sup>S. Wada, et al., "Enhanced Piezoelectric Property of Barium Titanate Single Crystals with Engineered Domain Configurations," *Jpn. J. Appl. Phys.*, **38** [Part 1, No. 9B] 5505–11 (1999).
- <sup>6</sup>G. L. Messing, et al., "Templated Grain Growth of Textured Piezoelectric Ceramics," *Crit. Rev. Solid State Mater. Sci.*, **29** [2] 45–96 (2004).
- <sup>7</sup>J. L. Jones, B. J. Iverson, and K. J. Bowman, "Texture and Anisotropy of Polycrystalline Piezoelectrics," *J. Am. Ceram. Soc.*, **90** [8] 2297–314 (2007).
- <sup>8</sup>A. B. Haugen, M. I. Morozov, J. L. Jones, and M.-A. Einarsrud, "Rayleigh Analysis of Dielectric Properties in Textured K<sub>0.5</sub>Na<sub>0.5</sub>NbO<sub>3</sub> Ceramics," *J. Appl. Phys.*, **116** [21] 214101–5 (2014).
- <sup>9</sup>N. Setter, et al., "Ferroelectric Thin Films: Review of Materials, Properties, and Applications," *J. Appl. Phys.*, **100** [5] 051606–46 (2006).

  <sup>10</sup>S.-H. Kim, et al., "Orientation Effects in Chemical Solution Derived
- <sup>10</sup>S.-H. Kim, et al., "Orientation Effects in Chemical Solution Derived Pb(Zr<sub>0.3</sub>,Ti<sub>0.7</sub>)O<sub>3</sub> Thin Films on Ferroelectric Properties," *Thin Solid Films*, **416** [1–2] 264–70 (2002).
- <sup>11</sup>H. Kuwabara, N. Menou, and H. Funakubo, "Strain and In-Plane Orientation Effects on the Ferroelectricity of (111)-Oriented Tetragonal Pb (Zr0.<sub>35</sub>Ti<sub>0.65</sub>)O<sub>3</sub> Thin Films Prepared by Metal Organic Chemical Vapor Deposition," *Appl. Phys. Lett.*, **90** [22] 222901–3 (2007).
- <sup>12</sup>H. Kuwabara, N. Menou, and H. Funakubo, "1 V Saturated Pb(Zr,Ti)O<sub>3</sub> Films with (111) Orientation Using Lattice-Matched (111)SrRuO<sub>3</sub>/(111)Pt Bottom Electrode Prepared by Pulsed Metal Organic Chemical Vapor Deposition," *Appl. Phys. Lett.*, **93** [15] 152901–3 (2008).
- <sup>13</sup>A. Mazzalai, D. Balma, N. Chidambaram, R. Matloub, and P. Muralt, "Characterization and Fatigue of the Converse Piezoelectric Effect in PZT Films for MEMS Applications," *J. Microelectromech. S.*, **24** [4] 831–8 (2015).
- <sup>14</sup>M. Wallace, et al., "In Situ Measurement of Increased Ferroelectric/Ferroelastic Domain Wall Motion in Declamped Tetragonal Lead Zirconate Titanate Thin Films," J. Appl. Phys., 117 [5] 054103–8 (2015).
  <sup>15</sup>F. Griggio, et al., "Substrate Clamping Effects on Irreversible Domain
- <sup>15</sup>F. Griggio, et al., "Substrate Clamping Effects on Irreversible Domain Wall Dynamics in Lead Zirconate Titanate Thin Films," *Phys. Rev. Lett.*, **108** [15] 157604-5 (2012).
   <sup>16</sup>F. Xu, S. Trolier-McKinstry, W. Ren, B. Xu, Z.-L. Xie, and K. J. Hem-
- <sup>16</sup>F. Xu, S. Trolier-McKinstry, W. Ren, B. Xu, Z.-L. Xie, and K. J. Hemker, "Domain Wall Motion and Its Contribution to the Dielectric and Piezoelectric Properties of Lead Zirconate Titanate Films," *J. Appl. Phys.*, 89 [2] 1336–48 (2001).
- <sup>17</sup>J. L. Jones, M. Hoffman, J. E. Daniels, and A. J. Studer, "Direct Measurement of the Domain Switching Contribution to the Dynamic Piezoelectric Response in Ferroelectric Ceramics," *Appl. Phys. Lett.*, 89 [9] 092901–3 (2006).
   <sup>18</sup>M. O. Eatough, D. Dimos, B. A. Tuttle, W. L. Warren, and R. Ramesh,
- <sup>18</sup>M. O. Eatough, D. Dimos, B. A. Tuttle, W. L. Warren, and R. Ramesh, "A Study of Switching Behavior in Pb(Zr,Ti)O<sub>3</sub> Thin Films Using X-Ray Diffraction." *MRS Proc.*, **361**, 111 (1994).
- Diffraction," MRS Proc., **361**, 111 (1994).

  <sup>19</sup>B. A. Tuttle, et al., "Chemically Prepared Pb(Zr,Ti)O<sub>3</sub> Thin Films: The Effects of Orientation and Stress"; ISAF '92 Proc. Eighth IEEE Int. Symp. Appl. Ferroelectr., 1992.
- <sup>26</sup>K. S. Lee, Y. K. Kim, S. Baik, J. Kim, and I. S. Jung, "In Situ Observation of Ferroelectric 90°-Domain Switching in Epitaxial Pb(Zr, Ti)O<sub>3</sub> Thin Films by Synchrotron X-ray Diffraction," Appl. Phys. Lett., **79** [15] 2444–6 (2001).
- <sup>21</sup>R. L. Johnson-Wilke, et al., "Ferroelectric/Ferroelastic Domain Wall Motion in Dense and Porous Tetragonal Lead Zirconate Titanate Films," *IEEE Trans. Ultrason. Ferroelectr. Freq. Control.* **62** [1] 46–55 (2015).
- IEEE Trans. Ultrason. Ferroelectr. Freq. Control, **62** [1] 46–55 (2015).

  <sup>22</sup>T. Yamada, et al., "Negligible Substrate Clamping Effect on Piezoelectric Response in (111)-Epitaxial Tetragonal Pb(Zr, Ti)O<sub>3</sub> Films," J. Appl. Phys., **118** [7] 072012–6 (2015).
- <sup>23</sup>G. Tutuncu, B. Li, K. Bowman, and J. L. Jones, "Domain Wall Motion and Electromechanical Strain in Lead-Free Piezoelectrics: Insight from the Model System (1 x)Ba(Zr<sub>0.2</sub>Ti<sub>0.8</sub>)O<sub>3</sub>–x(Ba<sub>0.7</sub>Ca<sub>0.3</sub>)TiO<sub>3</sub> Using *In Situ* High-Energy X-ray Diffraction During Application of Electric Fields," *J. Appl. Phys.*, 115 [14] 144104–7 (2014).

  <sup>24</sup>J. L. Jones, E. B. Slamovich, and K. J. Bowman, "Domain Texture Distri-
- <sup>24</sup>J. L. Jones, E. B. Slamovich, and K. J. Bowman, "Domain Texture Distributions in Tetragonal Lead Zirconate Titanate by X-ray and Neutron Diffraction," *J. Appl. Phys.*, **97** [3] 034113–6 (2005).
- <sup>25</sup>M. Kohli, P. Muralt, and N. Setter, "Removal of 90° Domain Pinning in (100) Pb(Zr<sub>0.15</sub>Ti<sub>0.85</sub>)O<sub>3</sub> Thin Films by Pulsed Operation," *Appl. Phys. Lett.*, **72** [24] 3217–9 (1998).
- <sup>26</sup>N. Tohge, S. Takahashi, and T. Minami, "Preparation of PbZrO<sub>3</sub>-PbTiO<sub>3</sub> Ferroelectric Thin Films by the Sol-Gel Process," *J. Am. Ceram. Soc.*, **74** [1] 67–71 (1991).
- $^{27}$ N. Ledermann, et al., "{100}-Textured, Piezoelectric Pb( $Zr_x$ ,  $Ti_{1-x}$ )O<sub>3</sub> Thin Films for MEMS: Integration, Deposition and Properties," *Sensor. Actuat. A Phys.*, **105** [2] 162–70 (2003).
- <sup>28</sup>A. P. Hammersley, S. O. Svensson, M. Hanfland, A. N. Fitch, and D. Hausermann, "Two-Dimensional Detector Software: From Real Detector to Idealised Image or Two-Theta Scan," *High Press. Res.*, **14** [4–6] 235–48 (1996)
- (1996).

  29 JCPDS Card International Centre for Diffraction Data<sup>®</sup>, 01–070–4261.
- <sup>30</sup>A. Pramanick, D. Damjanovic, J. E. Daniels, J. C. Nino, and J. L. Jones, "Origins of Electro-Mechanical Coupling in Polycrystalline Ferroelectrics During Subcoercive Electrical Loading," *J. Am. Ceram. Soc.*, **94** [2] 293–309 (2011). □

Copyright of Journal of the American Ceramic Society is the property of Wiley-Blackwell and its content may not be copied or emailed to multiple sites or posted to a listserv without the copyright holder's express written permission. However, users may print, download, or email articles for individual use.